Journal of Cultural Heritage 77 (2026) 341–350

Contents lists available at ScienceDirect

Journal of Cultural Heritage

journal homepage: www.elsevier.com/locate/culher

Original article

Assessment and characterization of *Origanum vulgare* essential oil in highly viscous polymeric dispersions for cleaning cultural heritage stone materials

Laura Giuliani[a,1], Chiara Genova[b,1], Elisa Villani[a,1], Valeria Stagno[a,1], Luca Paoletti[c,1], Ekaterina Oknazova[b,1], Alessandro Ciccola[b,1], Damiana Magris[d,2], Clive Cruickshank[d,2], Gabriele Favero[b,1], Dave J. Adams[e,3,*], Silvia Capuani[f,g,3,*]

[a] *Department of Earth Sciences, Sapienza University of Rome, Italy*
[b] *Department of Environmental Biology, Sapienza University of Rome, Italy*
[c] *Department of chemistry and technologies of drug, Sapienza University of Rome, Italy*
[d] *Historic Environment Scotland, UK*
[e] *School of Chemistry-University of Glasgow, UK*
[f] *National Research Council Institute for Complex Systems (CNR-ISC) c/o Physics Department, Sapienza University of Rome, Italy*
[g] *NeuroImaging Laboratory, Santa Lucia Foundation, 00179, Rome, Italy*

ARTICLE INFO

Article history:
Received 24 March 2025
Accepted 15 December 2025

Keywords:
Highly viscous polymeric dispersions (HVPDs)
Origanum vulgare essential oil
Carvacrol
Stone biodeterioration
^{1}H NMR

ABSTRACT

Stone biodeterioration caused by microbial colonisation poses significant challenges to the conservation of cultural heritage. Here, we investigate highly viscous polymeric dispersions (HVPDs) using *Origanum vulgare* essential oil (EO) and its primary active component, carvacrol, to provide an eco-friendly alternative to conventional chemical biocides. The formulations were characterised by rheology, revealing shear-thinning behaviour that facilitates both application and subsequent peeling removal. Proton Nuclear Magnetic Resonance spectroscopy (^{1}H NMR) provided insights into the chemical interactions and molecular dynamics within the HVPDs. Both HVPDs formulations with EO and carvacrol were applied to remove biofilm from a sandstone surface at Castlelaw, an ancient Iron Age fort in Scotland. Biocidal efficacy was assessed through Adenosine triphosphate (ATP) bioluminescence assays, showing substantial reductions in microbial contamination, and Fourier Transformed infra-red spectroscopy (FTIR ATR) highlighted the removal of biogenic compounds. Both formulations maintained significant antimicrobial activity over two months, suggesting their potential for long-term application in conservation. Overall, this study underscores the viability of HVPDs enriched with natural essential oils as sustainable solutions for microbial biodeterioration in historic stone materials, paving the way for future advancements in conservation practices.

1. Introduction and research aim

Stone biodeterioration is a pressing concern in the preservation of cultural heritage, as historic monuments are particularly vulnerable to microbial colonization [1–3]. Biofilms formed by bacteria, fungi, algae, and lichens can cause both aesthetic damage, such as discoloration, and deeper structural deterioration [4–6]. These microorganisms produce organic acids that contribute to the dissolution of stone minerals, while moisture cycles can induce mechanical stress, leading to cracks and flaking. [6] Furthermore, biofilms trap moisture, increasing the porosity of the stone and making it more susceptible to freeze-thaw cycles and salt crystallization [7,8].

* Corresponding authors.
E-mail addresses: laura.giuliani@uniroma1.it (L. Giuliani), chiara.genova@uniroma1.it (C. Genova), elisa.villani@uniroma1.it (E. Villani), valeria.stagno@uniroma1.it (V. Stagno), luca.paoletti@uniroma1.it (L. Paoletti), oknazova.2047685@studenti.uniroma1.it (E. Oknazova), alessandro.ciccola@uniroma1.it (A. Ciccola), damiana.magris@hes.scot (D. Magris), clive.cruickshank@hes.scot (C. Cruickshank), dave.adams@glasgow.ac.uk (D.J. Adams), silvia.capuani@roma1.infn.it (S. Capuani).
[1] Present/permanent address: P.le Aldo Moro 5, 00185 Rome, Italy.
[2] Present/permanent address:Longmore House, Salisbury Place, Edinburgh, EH9 1SH.
[3] Present/permanent address: Glasgow, G12 8QQ, Scotland.

https://doi.org/10.1016/j.culher.2025.12.008

Traditional methods for biofilm removal from stone surfaces often involve chemical biocides such as benzalkonium chloride, Preventol RI 50, RI 80 [9–13]. While effective, these compounds carry significant drawbacks, including toxicity to the environment, potential damage to the stone, and the risk of promoting microbial resistance [9–13]. In addition, repeated applications can compromise the material's aesthetic and structural integrity [9–13].

To address these limitations, the use of essential oils (EO, e.g.) as natural biocides confined within highly viscous polymeric dispersions (HVPDs) [9–11,14–17] was investigated. Essential oils, particularly *Origanum vulgare*, are known for their antimicrobial properties and can offer a more environmentally friendly alternative to synthetic biocides [9,10,18–20]. The primary active compound in *Origanum vulgare* EO, carvacrol, is effective against a broad spectrum of microorganisms, disrupting microbial cell membranes and inhibiting growth [9,10,15,18,21]. Carvacrol exerts its biocidal action by compromising the structure of microbial cell membranes [21], by altering membrane permeability and leading to the loss of essential intracellular components such as ions and ATP [9,10,17]. This mechanism results in metabolic dysfunction, which in turn inhibits the growth and proliferation of microorganisms [22,23].

Genova et al. highlight that the use of carvacrol and *Origanum vulgare* within a gel matrix ensures a homogeneous distribution of the biocidal [10] also reducing their volatility, a characteristic that could represent a potential limitation of these substances [24,25]. Such aspects are crucial for providing prolonged and controlled release over time, which is essential for combating microbial resistance and minimising the recolonisation of treated surfaces [9,10,18–20].

In this study, we investigate and characterize *Origanum vulgare* EO and carvacrol incorporated into HVPDs based on polyvinyl alcohol (PVA) and borax [26] and test the biocidal effect on a sandstone surface at Castlelaw, an ancient Iron Age fort in Scotland. While previous studies [9,10,18–20] have explored the antimicrobial potential of EO in gel formulations, challenges remain in optimizing their delivery for prolonged efficacy. One key limitation is the volatility of EO, which can lead to a rapid decrease in biocidal activity over time. The hypothesis in this work is that HVPDs provide a structured polymeric matrix that could enhance EO stability, modulate its diffusion, and minimize undesirable interactions with the treated stone surface, and reducing the risk of microbial resistance. HVPDs were chosen for this study because they can form a highly viscous, cross-linked polymer network capable of stabilizing and potentially controlling the release of biocidal agents [27–30]. By assessing the structural and mechanical properties together with the biocidal effectiveness of these formulations on biocolonized sandstone surfaces, we aim to show their potential for application in the conservation of stone heritage. We underline that in this study, no microbiological identification was performed; however, the term 'biofilm' is used based on the presence of characteristic chemical components detected by FTIR and the visual appearance of the colonized surfaces.

2. Material and methods

2.1. Synthesis of HVPDs

Polyvinyl alcohol (PVA), with a molecular weight of 47,300 kDa and a hydrolysis degree of 80–90 %, supplied by Sigma Aldrich (St. Louis, MO, USA) and di-sodium tetra-borate decahydrate (Borax, B), purchased from AppliChem (Ottoweg, Germany), were used to synthetise HVPDs formulation. Commercial *Origanum vulgare* EO was obtained from Essenthya - Oli Essenziali Professionali (Cesena, Italy), while carvacrol were sourced from Sigma Aldrich (St. Louis, MO, USA). The synthesis was conducted at room temperature using a magnetic stirrer placed on a heating plate. A 6 % w/w borax stock solution was prepared in distilled water. Each formulation was obtained by dissolving 4 % w/w PVA in distilled water, followed by the addition of 2 % w/w additive (EO or carvacrol) and enough of the borax stock solution to achieve a final borax concentration of 0.5 % w/w, under continuous stirring. The total mass of each formulation was adjusted with distilled water to 100 % w/w. To fully dissolve the PVA in water, the mixture was heated to 90 °C with continuous stirring until a homogeneous and transparent solution was formed. In each case, after obtaining a clear 4 % w/w PVA aqueous solution, the specific additive was introduced, turning off the heat source, followed by the addition of a borax aliquot. For all formulations, the PVA/borax ratio was kept constant (PVA:B = 4.0:0.5 w/w %). The concentrations of EO and carvacrol were chosen based on information from relevant literature [9,10,14]. Table 1 summarises the final composition of each formulation.

Table 1
Composition of HVPD formulations prepared with a fixed PVA/borax ratio (4.0:0.5 w/w%) and varying concentrations of additives. All components are expressed as weight percent (w/w%).

Code	PVA (w/w %)	B (w/w %)	EO (w/w %)	Carvacrol (w/w %)
HVPD	4.0	0.5	-	-
HVPD+EO	4.0	0.5	2.0	-
HVPD+C	4.0	0.5	-	2.0

2.2. Rheology

The rheological properties of HVPD formulations were measured with a stress-controlled rheometer (TA Discovery HR1) to gauge their effectiveness in application and peel-based removal from stone surfaces. Roughly 800 μL of each sample was held at a constant temperature of 25 °C in the rheometer's thermostatic chamber for 2 h before testing. Flow and frequency sweep tests were carried out using a serrated aluminium plate-plate setup with a 20 mm diameter and a 500 μm working gap. Data collection and analysis were performed with TRIOS software (version 4.3.0.38388).

2.3. ^{1}H NMR spectroscopy

Proton NMR conventional and diffusion-weighted spectra were recorded at 25 °C on a 9.4T Bruker Avance-400 spectrometer. The spectrometer was equipped with a Bruker probe capable of generating magnetic field gradients along the x, y, and z axes with a maximum gradient strength of 1200 mT/m and equipped with a 10 mm diameter radiofrequency (rf) coil. The proton resonance frequency was 400.15 MHz, and Topspin 2.1 software was used for both data acquisition and spectral analysis.^{1}H spectra were referenced to the OH peak of H_2O at 4.73 ppm. Conventional ^{1}H spectra were obtained using the zg acquisition setup with the following parameters: 90° hard rf pulse width of 10 μs, acquisition window of 2.8 s, 10 s recycle delay, 16 scans, and 32 K data points. Diffusion-weighted spectra were collected using a Pulsed Gradient Stimulated Echo (PGStE) sequence, with parameters set as follows: 90° hard rf pulse width of 10 μs, diffusion time (Δ) equal to 260 ms, magnetic field gradient pulse duration (δ) equal to 3 ms along the x direction and gradient strength (g) set to 80 % of the maximum value. [31] The acquisition window was 2.8 s, with a recycle delay of 10 s, 256 scans, and 32 K data points.

^{1}H NMR spectra were collected with both conventional and diffusion-weighted (DW) NMR. The DW approach helped to strongly reduce the dominant OH water resonance, which obscures the -OH signals of HVPD potentially involved in crosslinking between PVA chains and retaining EO and carvacrol. All ^{1}H NMR

analyses of the HVPDs were performed using water as the solvent, with the water resonance at 4.7 ppm used as the internal reference. EO and carvacrol were analysed in their pure form, without any solvent, using the resonance at 4.7 ppm as the internal reference.

2.4. FTIR ATR

Fourier Transform Infrared (FTIR) spectra were collected at room temperature using an Alpha II Bruker spectrophotometer for the characterization of the HVPDs and a Nicolet iS50 FT-IR for the analysis of HVPDs formulations tested on the case study. Both the spectrometers were equipped with an Attenuated Total Reflection (ATR) probe, constituted by a platinum diamond crystal. The spectra were recorded with 32 scans and a resolution of 4 cm^{-1}, then processed with the software Origin. For every sample, three spectra were acquired through the mentioned set conditions and then averaged. HVPD formulations containing EO and carvacrol were examined both before and after application on stone surfaces to assess any potential chemical interactions with the degraded materials being treated. The FTIR-ATR spectra were collected on the HVPD films as fresh, after 24 h drying and after peeling from the stone surfaces. This approach allowed the identification of organic residues transferred from the biofilm to the gel during the cleaning process, providing indirect evidence of biofilm removal without direct sampling of the stone substrate.

2.5. Context and application cleaning tests on cultural heritage stone materials

Castlelaw Hillfort, situated in the Pentland Hills near Edinburgh, Scotland, is a historic Iron Age site, with initial occupation estimated between 500 BC and 500 AD. A key feature of the site is the "souterrain," a subterranean passage believed to have served purposes such as storage or security. For this study, four areas within the souterrain were selected based on their surface geometry and exposure to environmental factors. Two areas, characterized by curved profiles and limited sunlight exposure, did not yield significant results, while the other two areas, with flat surfaces, provided suitable conditions for the experimental procedures (Fig. 1). The applications of soft matter were conducted on 22, 24, and 25 July 2024. Temperature values (converted to Celsius) and relative humidity (RH) levels were obtained from the Weather Underground database. The average values and standard deviations are provided in Table 2. To contextualize these observations, additional climatic data from Weather Underground for Pentland Hills, Scotland, were considered. The site experiences average summer temperatures ranging from 10 °C to 17 °C, with July typically being the warmest month. In contrast, winter temperatures range from 0 °C to 5 °C. These data suggest that the experimental conditions during July could be representative of the local summer climate. However, it is important to note that the souterrain's subterranean environment likely stabilizes humidity and temperature compared to external conditions.

Fig. 1. The red arrows mark the specific areas in the underground environment where the HVPD formulations were applied.

Table 2
Environmental conditions at Castlelaw Hill Fort (Pentland Hills, Scotland) were recorded on date: 22nd, 23rd, 24th, and 25th July 2024. Temperature (°C) and relative humidity (RH %) values were retrieved from Weather Underground [32] and are presented as averages with standard deviations. These parameters are crucial for understanding the drying dynamics of the HVPD formulations. On 23rd July, due to persistently high relative humidity and limited air circulation within the hypogeal environment, the drying of the gels was incomplete after 24 h, and the contact time for the second application was therefore extended by an additional 24 h (total drying time: 48 h).

Date	T_{max}±SD °C	T_{min}±SD °C	RH_{max}±SD %	RH_{Min}±SD %
22	18.9 ± 0.6	12.2 ± 0.7	100 ± 3	73 ± 6
23	20.0 ± 0.6	12.8 ± 0.7	100 ± 3	64 ± 6
24	21 ± 1.	11.1 ± 0.7	100 ± 3	60 ± 6
25	19± 1.	12.2 ± 0.7	94 ± 3	64 ± 6

The investigated substrate is sandstone, forming the walls of the souterrain and covered with a biofilm layer. Although no microbiological or genomic analyses were conducted to identify the microbial species involved, the presence of a biofilm was inferred from both the macroscopic appearance of the colonized surfaces and the FTIR-ATR spectra, which revealed characteristic signals of proteins, polysaccharides, lipids and nucleic acids. The dark-green to black coloration observed suggests that the colonization is most likely photosynthetic in nature, involving algae, cyanobacteria, or lichens. The biocidal efficacy observed in this study indicates that such organisms are susceptible to treatments based on Origanum vulgare EO and carvacrol.

The formulations were applied twice consecutively using a spatula and left to dry for 24 h. After the drying period, the HVPDs were removed by peeling.

Each area was treated with two consecutive applications of the HVPD formulations. During the first test, a 24-hour contact time was sufficient to allow complete drying and easy removal of the gels by peeling. However, for the second application, the drying period was extended to 48 h. This adjustment was necessary because of the variable microclimatic conditions typical of the hypogeal environment at Castlelaw Hillfort, where high relative humidity and limited air circulation delayed the evaporation of water from the gels and prevented complete drying within 24 h. Despite these constraints, both formulations were successfully removed without leaving visible residues, confirming their applicability even under suboptimal environmental conditions.

This application methodology was refined through two preliminary tests. All the HVPDs were applied on an outdoor biocolonized travertine surface to optimize the application procedure (see Supplementary materials, figure S8). Since the HVPD base formulation (without EO or carvacrol) showed poor peelability and biocidal properties, a further test provided its application on a sandstone sample to better assess its removal behaviour. Even in this case, the peeling process resulted in poor detachment and the formation of visible polymeric residues on the stone surface, indicating limited reversibility and unsuitability for practical use. A representative image of this result is provided in the Supplementary Materials (Figure S9). Therefore, to minimize residues and optimize peeling, we relied on our previous work [26], which suggested how to change the viscoelasticity of the soft matter to minimize residue formation. Consequently, the base HVPD formulation was excluded from testing on the historical site to avoid any risk of surface alteration.

2.6. Monitoring of the biocidal action and its chemotype by bio-luminometer

The biocidal efficacy of HVPDs loaded with EO and carvacrol was assessed using the Hygiena® SystemSURE Plus bioluminometer in conjunction with SuperSnap® High Sensitivity ATP Surface Test. This system measures ATP (adenosine triphosphate) levels on surfaces, which indicate organic contamination, both before and after treatment. 28,29 The bio-luminometer can detect down to 1 femtomole (1 × 10–15 mol) of ATP, in particular, the instrument has a limit of detection of 0.1 fmol. For each area, three separate measurements were taken to ensure accuracy and reliability. For sampling, a SuperSnap® swab was used.

3. Results and discussion

3.1. Characterisation of HVPD

In the first step, ^{1}H NMR spectra of HVPDs using conventional and DW spectra were obtained to check the possibility of observing -OH resonances of HVPD (Fig. 2). Based on the cross-linking between PVA and borax, this soft matter establishes a complex network of interactions. In Fig. 2, focusing on the red conventional NMR spectrum, the enormously intense resonance centred at 4.73 ppm belongs to water. The wide resonance at approximately 1.5 ppm is attributed to the methylene protons (-CH_2) of the PVA structure [33,34], indicating a well-organised segment of the polymer chain. Around 3.9 ppm, the main -CH resonance is observed, and at 4.3 and 3.5 ppm, the hydroxyl (-OH) groups of PVA, specifically those located on the polymer backbone and side chains [35,36]. These hydroxyl groups represented by a narrow resonance are primarily involved in a rapid chemical exchange with water OH and do not interact by hydrogen bonds with borax or other PVA chains. Due to the rapid dynamics, the signals at 4.3 and 3.5 ppm are not visible in the DW spectrum where diffusion weight selects slower dynamics than that of free water.

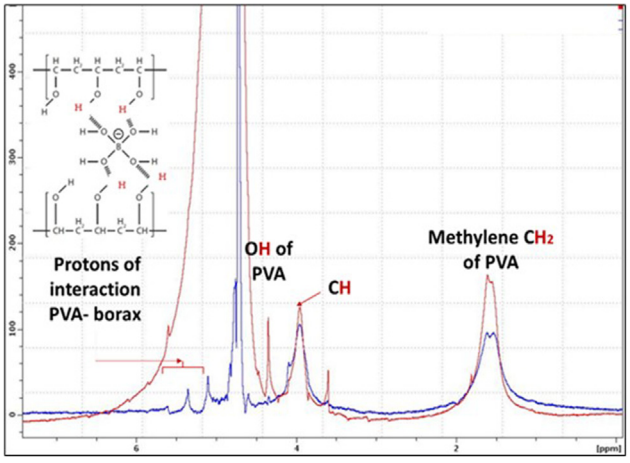

Fig. 2. The ^{1}H NMR conventional spectrum (shown in red) and DW spectrum (in blue) of HVPD. In both spectra, two prominent resonances are observed: methylene protons (-CH_2) at around 1.5 ppm and methine protons (-CH) at 3.9 ppm. In the red spectrum, a large water resonance is visible between 4.5 and 6 ppm, along with the -OH resonances of PVA that do not interact with other PVA chains or borate ions. In the blue spectrum, additional resonances provide more detailed insights into the interactions between PVA and borax. Specifically, distinct -OH resonances appear in the 5–6 ppm range (notably at 5.1, 5.3, and 5.6 ppm), which can be attributed to the protons of PVA involved in interactions with borate ions. The resonances at 4.3 and 3.5 ppm, by contrast, are likely associated with -OH groups of PVA that do not interact with borate ions. The resonance at 4.7 ppm is used as the internal reference.

When the water signal is strongly reduced (blue DW spectrum in Fig. 2), previously hidden resonances emerge, clarifying the interactions between PVA chains and tetrahydroxyborate. Specifically, resonances around 5.1, 5.3, 5.6 ppm become visible. They are associated with -OH groups of PVA engaged in interactions (hydrogens bond) with $[B(OH)_4]^-$. These interactions form cross-bridges between PVA chains, indicating the role of tetrahydroxyborate in creating a highly viscous, complex polymer network [33,34,37–39]. This network is crucial for the mechanical stability of the formulation. ^{1}H–NMR measurements were also performed on PVA in aqueous solution to identify the polymer resonances comparing them with those obtained upon the addition of borax. The ^{1}H–NMR spectra of PVA in aqueous solution, compared with those of HVPD, are provided in the Supplementary materials (Figures S1, S2).

Fig. 3 illustrates the dynamic viscosity as a function of shear rate and presents the oscillatory frequency sweep analyses for HVPD, HVPD+EO, and HVPD+C. All formulations exhibit a pronounced shear-thinning behaviour, a characteristic feature of polymeric dispersions [26,40,41]. In the steady shear tests, at low shear rates the high viscosity reflects a highly entangled or densely cross-linked polymer network—likely stemming from borax-induced physical cross-links between PVA chains. However, measurements at shear rates below 10^{-3} s^{-1} should be interpreted with caution, as these values may be affected by low torque limitations and thus could represent experimental artifacts. To further assess data quality, a shear stress versus shear rate plot (not shown) confirmed the expected non-Newtonian behaviour, although at high shear rates the viscosity tends to stabilize around 1000 Pa·s, indicating a resistance to flow under moderate deformation.

For the oscillatory tests, amplitude sweep experiments were initially performed to define the linear viscoelastic region. All frequency sweep measurements reported here were conducted within this linear regime (at shear strains typically below 1 %, as determined by preliminary tests), ensuring that the elastic (G′) and viscous (G″) moduli accurately reflect the intrinsic viscoelastic behaviour of the systems.

The incorporation of EO or carvacrol significantly modifies the viscosity profiles. In particular, HVPD+C exhibits the lowest viscosity at high shear rates, suggesting that carvacrol may slightly disrupt the polymer network, thereby enhancing fluidity. Importantly, this increased fluidity under strong deformation can be beneficial for practical applications, as it may facilitate spreading, penetration into surface irregularities, and subsequent removal of the gel. This shear-thinning response at high deformation does not necessarily reflect the small-deformation elasticity of the system, which is instead captured by the oscillatory moduli discussed below.

Conversely, HVPD+EO retains a slightly higher viscosity, likely due to stronger interactions between the essential oil components and the hydroxyl as well as borate groups in the PVA matrix, which contribute to a more cohesive and stable network. Pure HVPD, without additives, demonstrates the highest viscosity, indicative of a more densely cross-linked structure.

The shear stress vs shear rate graph (Figure S7-Supplementary materials) provides key insights into the rheological behaviour of the HVPDs and their modified formulations.

Regarding the viscoelastic properties (Figs. 3b–3d), at low frequencies, the loss modulus (G″) predominates, while at higher frequencies the storage modulus (G′) exceeds G″, signalling a transition towards elastic behaviour. The apparent relaxation time (τc) was determined from the crossover region of the moduli curves and by fitting the terminal region of the frequency sweep data. This parameter has been calculated as reported by Giuliani et al. [26]. For pure HVPD, τc is approximately 65 s, reflecting a network with long relaxation dynamics due to extensive cross-linking. In contrast, HVPD+EO exhibits a much shorter τc of about 12.6 s, in-

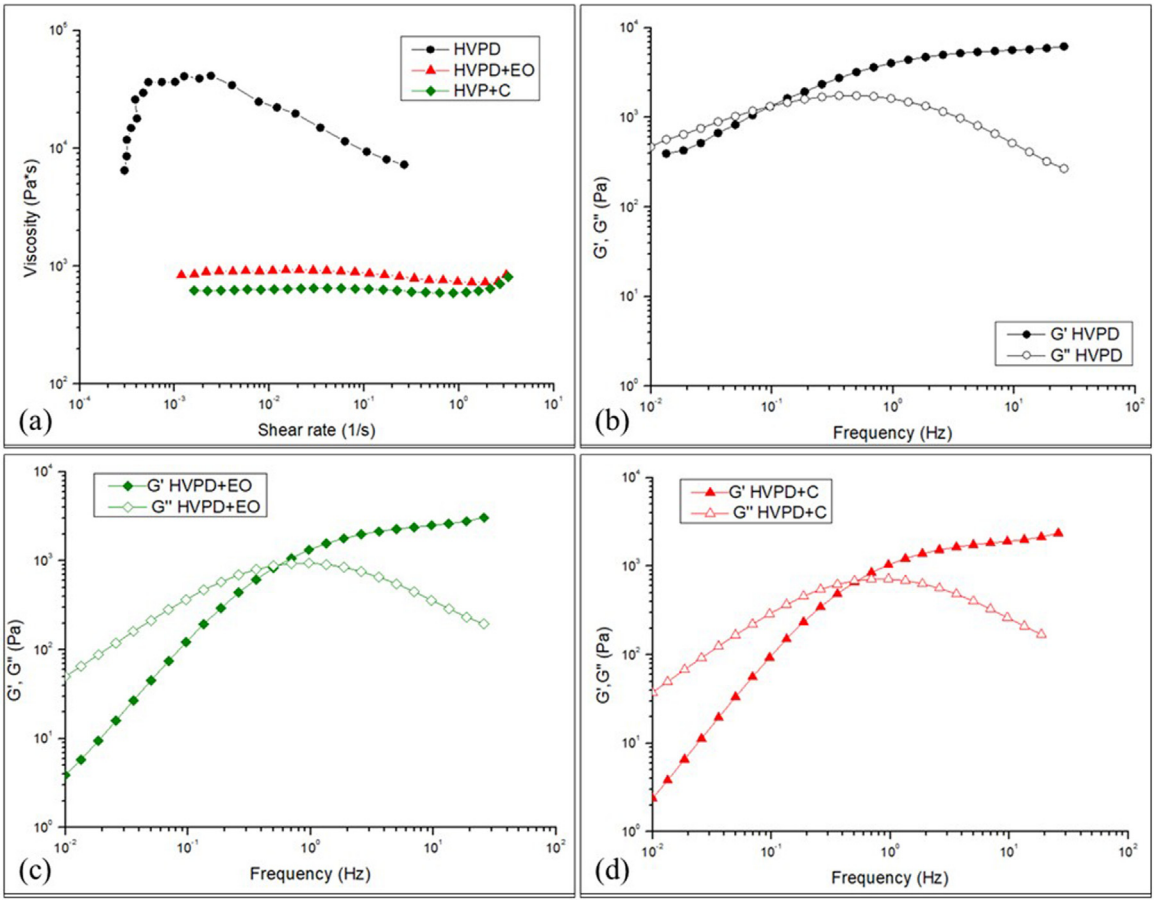

Fig. 3. (a) Flow curves of the dynamic viscosity as a function of the shear rate for HVPD (black line), HVPD+EO (green line), HVPD+C (red line), (b), (c), (d), log-log plot of storage modulus (G′) and loss modulus (G″) versus frequency for HVPD, HVPD+EO and HVPD+C, respectively.

dicative of a more fluid-like structure with a faster transition from viscous to elastic behaviour. HVPD+C shows an intermediate τc of approximately 10.5 s, suggesting that while carvacrol reinforces certain interactions, it still permits a relatively rapid viscoelastic response.

The flow curves did not reveal a clear yield stress for the formulations, which, together with the predominantly shear-thinning behaviour, may raise concerns regarding potential gravity-driven flow on vertical surfaces—a factor that should be considered in practical applications.

The "apparent elastic modulus" (G_n) reported in Fig. 4 was obtained by extrapolating the plateau region of the G′ versus frequency curve, as reported by Giuliani et al. [26]. As expected, neat

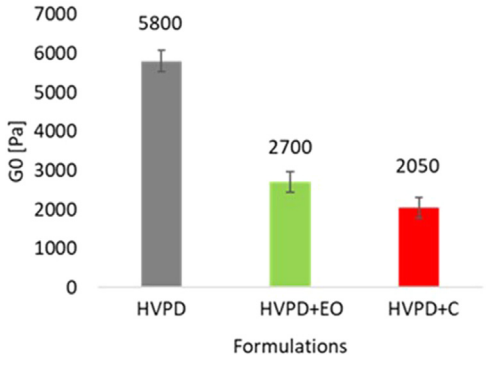

Fig. 4. Intrinsic elastic modulus G_0 of HVPD, HVPD+EO, HVPD+C.

HVPD exhibits the highest G_n, consistent with a densely cross-linked network. The incorporation of carvacrol results in the lowest G_n, indicating a pronounced softening effect and a reduction in the elastic integrity of the network. HVPD+EO displays an intermediate G_n.

Although peeling is primarily governed by the adhesive interactions between HVPD and the sandstone substrate, the viscoelastic properties of the formulations may indirectly influence removal performance. In this regard, the slightly higher G_n observed for HVPD+EO suggests a more elastic and cohesive gel network, whereas the reduced elasticity of HVPD+C is consistent with a softer and more deformable structure that may affect its detachment behaviour on highly adhesive surfaces. These observations highlight a potential interplay between viscoelasticity and adhesion, although the adhesion properties themselves require further investigation to fully elucidate the peeling mechanism.

While rheological measurements provide valuable insights into the viscoelastic behaviour of HVPDs, they do not directly quantify the encapsulation efficiency of the bioactive compounds. Nevertheless, based on the observed viscosity trends, it may be hypothesised that the polymeric network contributes to retaining the essential oil by limiting its diffusion and evaporation. Complementary studies, such as NMR analyses, are planned to further assess the encapsulation efficiency and molecular mobility of carvacrol and EO within the polymeric matrix.

In this regard, the observation of the broadening of some resonances in the HVPD+EO and HVPD+C NMR spectra, can indicate enhanced molecular interactions and/or slower dynamics. The resonance at 5.1, 5.3 and 5.6 ppm (Fig. 5(a)), associated with PVA-borax interactions in the HVPD spectrum, broadens in the

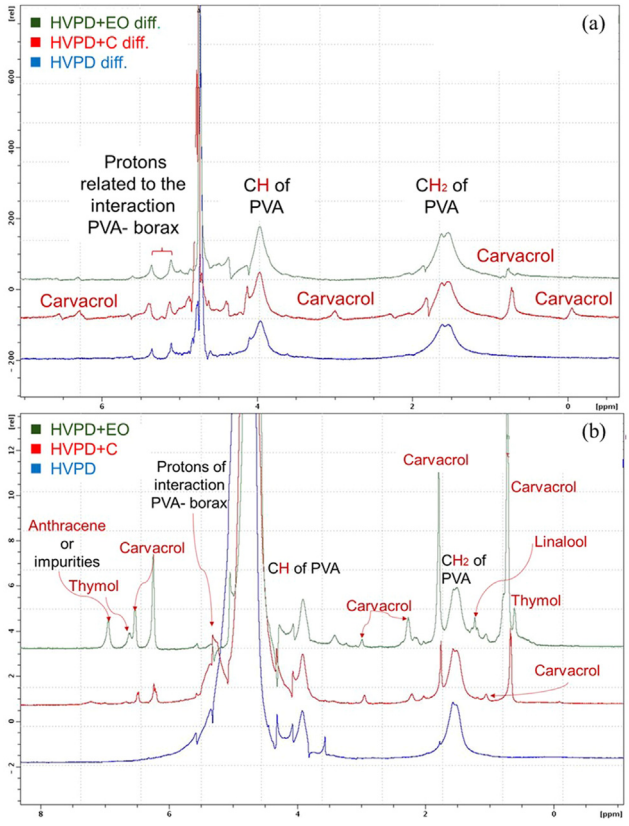

Fig. 5. ^{1}H NMR spectrum of HVPD (in blue), HVPD enriched with EO (HVPD+EO, in green), and HVPD enriched with carvacrol (HVPD+C, in red). In (a) and (b) are shown the spectrum with and without water diffusion suppression, respectively. Key assignments include protons related to the PVA- tetrahydroxyborate interaction, well visible in a), -CH and CH_2 protons of PVA, and characteristic resonances of carvacrol (see also supplementary materials) In the HVPD+EO sample, additional signals are observed, indicating impurities like anthracene and EO components such as thymol. The resonance at 4.7 ppm was used as the internal reference.

HVPD+EO and HVPD+C spectra, suggesting that the EO and carvacrol induce more complex interactions compared to those in HVPD formulation, likely driven by hydrogen bonding, with the polymer network. The half-height linewidths of resonances at 5.6, 5.3, and 5.1 ppm, quantify the interactions/dynamics within the system (see Histogram in Fig. 6). The broadening of these resonances indicates interactions between the hydroxyl groups of PVA

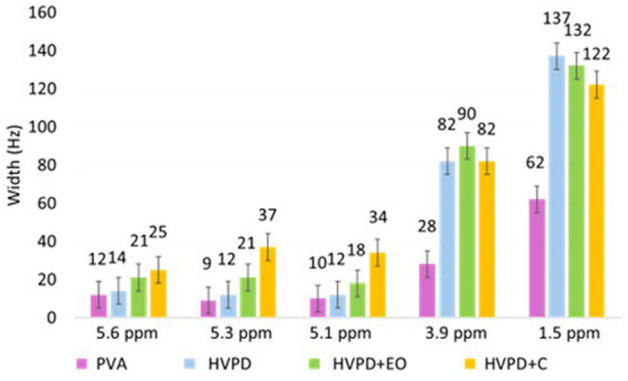

Fig. 6. Histogram comparing the linewidths of significant resonances at 5.6, 5.3, 5.1 ppm (-OH, PVA-B interaction), 3.9 (-CH, in PVA), 1.5 (-CH_2 in PVA) ppm, in the PVA formulation without borax (pink), HVPD (blue), HVPD +EO (green), HVPD +C (orange) spectra. The resonance widths provide insight into the molecular interactions within the polymer matrix, with broader resonances at 5.3 and 5.1 ppm, indicating enhanced interactions following the addition of carvacrol and EO.

and borax, with a significantly greater effect observed upon the addition of EO, as detailed in Fig. 6. In contrast, the resonances at 3.9 ppm and 1.5 ppm exhibit minimal changes in linewidth, as shown in Fig. 5(a).

The spectrum of HVPD+C (Fig. 5) is characterized by broader resonances at 5.6 ppm, 5.3 ppm, 5.1 ppm, 3.9 ppm, and 1.5 ppm compared to HVPD. This broadening, particularly for hydroxyl–associated signals, suggests that carvacrol might interact more strongly with the PVA-borax network than EO slowing down the overall dynamics of the system. Fig. 6 reports the line widths of resonances for all the formulations, started from PVA in water without borax (PVA), HVPD (blue), HVPD +EO (green), HVPD +C (orange).

A significant increase in the linewidth of the resonances due to the addition of borax compared to the formulation without the $[B(OH)_4]^-$ ion is evident. This is observed little in the resonances 5.1, 5.3, and 5.6 and much more in the resonances at 3.9 and 1.5, which are more affected by the presence of the quadrupolar nucleus of boron. Since the resonances at 1.5 and 3.9 ppm are characterized by slower dynamics, the protons -CH and -CH_2 are more affected by the relaxation induced by the quadrupolar nucleus [42–44].

With the addition of OE and carvacrol the lines at 1.5 ppm and 3.9 ppm within the measurement errors do not undergo variations in linewidth, while a trend of increase in the linewidth of the resonances at 5.1, 5.3, and 5.6 ppm is evident with the maximum linewidth for the formulation HVPD+C.

The broadening of NMR resonances—particularly those related to the hydroxyl groups involved in PVA–borax interactions—might indicate additional interactions introduced by the additives, especially carvacrol. However, this broadening may reflect a more complex and heterogeneous bonding environment. The additives could be promoting transient or varied hydrogen-bond interactions that disrupt the regularity of the cross-linked network. This disruption might result in a lower effective cross-link density, thereby producing a more fluid-like macroscopic behaviour, as evidenced by the reduced viscosity and shorter relaxation times in our rheological data. Further investigations are necessary to fully elucidate these multi-scale effects. Additional evidence supporting these interactions is provided by FTIR spectroscopy, which is included in the Supplementary Materials (Figure S3).

3.2. Evaluation of biocidal efficacy and removal performance of HVPD+EO and HVPD+C

In Areas 1 and 4 (Fig. 1), both HVPD+EO and HVPD+C were removed easily without leaving visible residues in the first application. After treatment and removal of the HVPD formulations, the stone surfaces appeared visually lighter. Although no instrumental colorimetric measurements (e.g., ΔE^*) were performed, this perceptible change is likely related to the removal of superficial biological patinas. Further spectro-colorimetric and surface analyses will be needed to determine whether this effect corresponds to a real chromatic alteration or to increased surface reflectance due to cleaning.

However, due to an increase in atmospheric humidity, the products did not completely dry in the second application. This made the peeling process more difficult, although, despite the adverse conditions, both formulations were still removed. Fig. 7 shows the condition of Area 1 before and after treatment.

In Areas 2 and 3, characterized by curved surfaces not exposed to direct sunlight, the products did not dry sufficiently after the first application. Due to atmospheric conditions, the drying time was extended to 48 h. However, with the rise in humidity, the peeling process became even more compromised. The products left macro-residues, making the test less reliable for these areas.

Table 3
Luminometer results express in RLU± standard deviation.

Area of application HVPDs	RLU±Dev.St. Pre-treatment	RLU±Dev.St. Post treatment	RLU±Dev.St. After two months
Area 1 EO	3571±1	4 ± 1	417±20
Area 1 C.	3571±1	4 ± 1	476±11
Area 4 EO	3789±1	18±11	711±4
Area 4 C.	3789±1	9 ± 2	781±103

The ATP data show a significant reduction in microbial contamination immediately after treatment, with both products achieving RLU levels considerably lower than the initial state.

This addition clarifies the challenges associated with drying times and residue removal in the study, which is important for discussing the practical implications of the formulations under real environmental conditions.

The biocidal activity of HVPD+EO and HVPD+C was assessed by measuring ATP levels on treated surfaces. The results are reported in Table 3.

In contrast to the preliminary tests on travertine, where the differences in the removal of the HVPDs were more evident (see SM), the application on the case study did not reveal substantial practical differences between HVPD+EO and HVPD+C. This discrepancy is likely related to the different environmental conditions: the high humidity recorded at Castlelaw Hill Fort (Table 2) probably contributed to a slower evaporation of water from the polymeric matrix. As a result, both HVPDs exhibited similar behaviour during application and peeling, despite their distinct viscoelastic characteristics measured in the laboratory. Nevertheless, this aspect warrants further investigation.

The variations observed in ATP reduction between HVPD+EO and HVPD+C (Table 3) are therefore attributed to the intrinsic antimicrobial activity of the incorporated compounds — Origanum vulgare essential oil and carvacrol — rather than to differences in their mechanical or viscoelastic characteristics.

Although the visual appearance of the treated areas (Fig. 7C–D) did not show evident recolonization after two months, the increase in ATP values (Table 3) suggests the early recovery of microbial metabolic activity. This apparent discrepancy can be attributed to the higher sensitivity of ATP bioluminescence measurements, which can detect biological activity at levels not yet visible on the surface.

This result is further confirmed by FTIR analysis, which reveals the effective removal of key biofilm components, including polysaccharides and proteins.

The supplementary materials include the FTIR-ATR spectra of HVPD (Figures S3), as well as the spectra of pure EO and carvacrol (Figures S6 a, b). In Fig. 8 and S3, the comparison of the HVPD formulation before and after 24 h (or fresh and dry) allows avoiding the signals attributable to the evaporation of free water, highlighting the PVA signals according to the literature [43]. For the fresh HVPDs, the main signals correspond to the O–H bending at 1640 cm-1 and the O–H stretching broad band around 3300 cm^{-1}, which can be assigned to the free water content, while minor signals at 1089 cm-1 and in the range 2800–3000 cm-1 are assigned to PVA C–O and C–H stretching, respectively. For the dry HVPD, instead, the band at 829 cm^{-1} is indicative of C–C stretching and C–H out-of-plane vibrations, while the signal at 919 cm^{-1} is attributable to CH2 stretching. The most intense band at 1089 cm^{-1} corresponds to C–O stretching, while the signals at

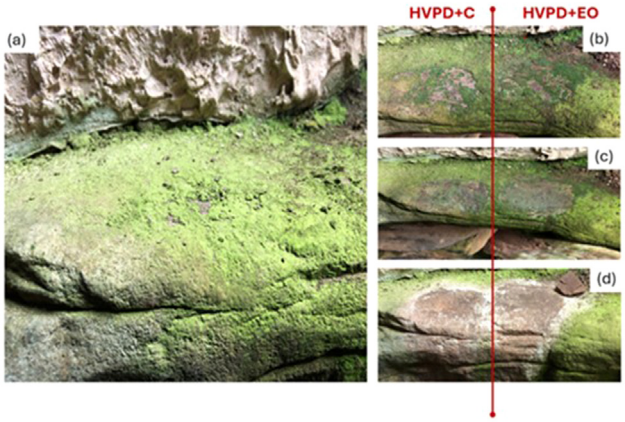

Fig. 7. First area treated with HVPD+EO and HVPD+C: (a) lithotype before treatment, (b) lithotype after the first application of HVPDs, (c) lithotype after two consecutive applications of HVPDs, (d) lithotype after two months from the treatments.

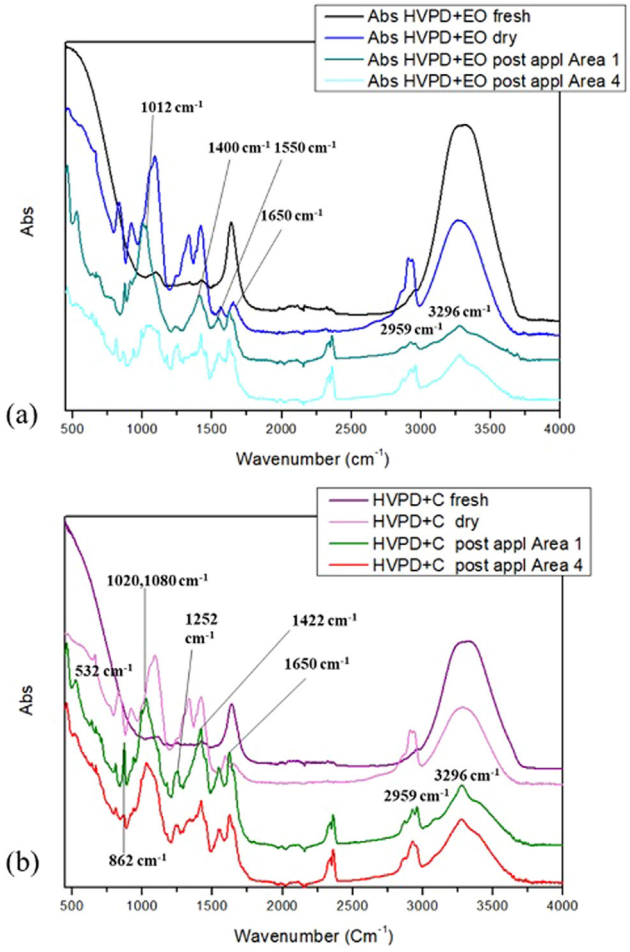

Fig. 8. FTIR spectra acquired after the application of HVPDs on the historical stone surface. (a) Spectra of HVPD+EO (fresh and dry) compared with the post-application residues collected from Areas 1 and 4. (b) Spectra of HVPD+C (fresh and dry) compared with the post-application residues collected from Areas 1 and 4. The spectra of the fresh and dry gels are shown for reference to highlight the main absorption bands of the polymeric matrix and to assist in the identification of the compounds removed (lipids, proteins, peptides). Characteristic wavenumbers (cm^{-1}) are indicated for clarity.

1242, 1335 and 1416 cm^{-1} could be assigned to CH_2 wagging, H–C-H and CH_2 bendings, respectively. The peak at 1592 cm^{-1} is attributable to the residual acetate groups deriving from manufacturing processes by poly vinyl acetate hydrolysis, while the band at 1653 cm^{-1} is assigned to O–H bending. The peaks at 2908 and 2937 cm^{-1} are attributed to C–H stretching, while the broad and intense band at 3270 cm^{-1} corresponds to O–H stretching. The spectral pattern presents a general correspondence with literature data [43] and this characterization granted for the proper evaluation of the applicative performances regarding the testing of HVPD+EO and HVPD+C formulations on the biodeteriorated surfaces of Castlelaw Hillfort. Fig. 8 shows the FTIR ATR spectra of HVPD+EO and HVPD+C, following their application, in comparison to the corresponding formulations as fresh and dried for 24 h, in order to highlight differences due to the evaporation of water and volatile species.

Specifically, in the case of HVPD+EO (Fig. 8a), both the formulations used for the on-site application highlight great changes in comparison to the fresh and dry HVPD, whose spectral pattern could be considered neglectable in the post-application spectra, because of the high intensity signals attributable to biological materials. A major difference corresponds to the rise of a broad band between 3200 and 3350 cm^{-1}, centred at approximately 3296 cm^{-1}. This band could be linked to Amide A, supporting the presence of microbial proteins in the biofilm matrix, while a peak at 2959 cm^{-1} associated with asymmetric CH_3 stretching vibrations -not visible in the case of the HVPD blank formulations-, could be attributed to the presence of lipids [45]. Another significant region, between 1500 and 1700 cm^{-1}, includes signals associated with carbonyl bonds (C=O), at 1703 cm^{-1}, but also amide I (1650 cm^{-1}) and II (1550 cm^{-1}) vibrations, which would support the presence of proteins and peptides [46,47]. These compounds are linked to microbial cells, algae, and fungi within the biofilm [46]. The high intensity of these peaks, particularly for HVPDs applied to area 4, may indicate a denser microbial colony in that region, characterized by strong protein and biological material production.

A critical band is observed between 1000 and 1200 cm^{-1}, where C–O-C (1020,1079 cm^{-1}) and C–OH (1116,1156 cm^{-1}) vibrations are characteristic of the sugar structure of polysaccharides within the biofilm, such as cellulose and other glucidic polymers [48–50]. These polysaccharides, common in microbial extracellular polymeric substances (EPS), accumulate in biodeteriorated areas, acting as a nutrient reservoir for bacteria and fungi. [51] These bands indicate that HVPD+EO effectively removed parts of the biofilm, pulling away both cellular and extracellular components contributing to stone degradation.

A critical aspect for biofilm identification is the peak observed around 1252 cm^{-1}, attributed to phosphate (P=O) groups, while the peak at 1012 cm^{-1} was attributed to C–C stretching vibrations in RNA and ribose. This set of signals is related to the presence of nucleic acids, cell membranes, and phosphorylated metabolites [52,53]. Finally, a peak at 862 cm^{-1} is observable, corresponding to (1→3), (1→6)-α-D-glucan structures. This suggests that HVPD+EO effectively removed a significant number of microbial cells.

The FTIR spectrum of HVPD+C in Figure 8(b), exhibits notable similarities to previous analyses; however, a significant increase in band intensity is observed within the 1400–1600 cm^{-1} region. The enhancement of the signal at 1422 cm^{-1}, likely attributable to C–H bending, suggests the presence of lipids, which are typically associated with microbial cell membranes. Moreover, distinct peaks at 1518 cm^{-1} and 1535 cm^{-1} can be attributed to the Amide II band, arising from N–H bending combined with C–N stretching vibrations, characteristic of protein structures [54]. The slight shift between these two peaks likely reflects variations in protein conformation.

Additionally, peaks at 1575 cm^{-1} and 1588 cm^{-1} correspond to the asymmetric stretching vibrations of the carboxylate group (COO^-) [55]. These signals are indicative of free fatty acids or carboxylate salts, potentially originating from oxidised lipids or components of the microbial extracellular matrix.

Further analysis of the 1000–1100 cm^{-1} region reveals characteristic vibrations associated with polysaccharides, such as cellulose and starch. These components are typical of algal and bacterial biofilms. Notably, prominent peaks around 1020 cm^{-1} and 1080 cm^{-1} further support the presence of polysaccharide-based biofilm materials on the treated surfaces [49–51,56].

These results show that HVPD+EO and HVPD+C act as cleaning agents, effectively removing the biofilm components responsible for the deterioration of stone surfaces. The combination of observations in dry and post-application samples underscores the potential of these formulations for cultural heritage conservation.

4. Conclusions

This study shows the successful integration of *Origanum vulgare* essential oil (EO) and carvacrol into highly viscous polymeric dispersions (HVPDs) based on polyvinyl alcohol (PVA) and borax, offering a sustainable approach for treating bio-colonized stone surfaces.

The characterisation of these formulations through complementary techniques, such as rheology and ^{1}H–NMR spectroscopy, provided key insights into their structural and functional properties, highlighting synergies between the methods. Rheological analyses revealed that all HVPD formulations exhibit shear-thinning behaviour, facilitating application on complex geometries and subsequent removal by peeling. The addition of EO reduced viscosity, enhancing fluidity, while carvacrol increased the elastic modulus (G′) and improved the viscoelastic balance, contributing to the structural stability of the HVPD system. These findings suggest that rheology effectively captures the mechanical adaptations induced by the incorporation of active compounds.

^{1}H–NMR spectroscopy complemented these findings by elucidating the molecular interactions within the polymer matrix. Resonances associated with hydroxyl groups (e.g., at 5.1, 5.3, and 5.6 ppm) broadened significantly in the presence of borax, confirming its role in cross-linking PVA chains. Upon the addition of EO or carvacrol, the spectra revealed differences in their interaction with the matrix: EO seems primarily to remain in solution with limited impact on the polymer structure, whereas carvacrol shows a more effective interaction with the PVA-borax network. This enhanced interaction was consistent with the increased rigidity observed in the rheological profiles of HVPD+C. Moreover, fifteen days after the preparation of HVPD+EO in the NMR tube, phase separation was observed between HVPD and EO. In contrast, no phase separation was detected in the NMR tube containing HVPD and carvacrol, even after one month of preparation.

Both rheology and ^{1}H–NMR techniques suggested that the HVPD formulations may be capable of incorporating and retaining active biocidal compounds, potentially enabling a gradual release over time, depending on the specific compound. These complementary findings also underscore the suitability of the PVA-borax network as a delivery system for antimicrobial agents. Biocidal efficacy was established through ATP bioluminescence assays, with significant reductions in microbial contamination observed immediately after treatment and sustained over two months. FTIR analyses further confirmed the removal of biofilm components, including polysaccharides and proteins, contributing to the preservation of the stone substrates. Future work will aim to integrate microbiological or metagenomic analyses to better characterise the microbial communities involved in stone biodeterioration. However, given the

objectives of this study—focused primarily on the chemical-physical characterization of cleaning formulations, their efficacy and the removal of microbial biomass—the chemical and structural indicators of biofilm presence were considered sufficient to evaluate treatment performance. Field challenges, such as high humidity at the Castlelaw Hill Fort site, showed how environmental and substrate variability can influence drying and removal. This highlights the need for adaptable application protocols and further targeted studies to refine performance across diverse conditions.

While no quantitative colorimetric or capillary water absorption tests were conducted in this study, no visible changes in colour or texture were observed following application and removal of the HVPD formulations. The products were designed for temporary application and peelable removal, minimizing the risk of long-term alteration or pore blockage. Nonetheless, further investigations on ΔE variation and permeability are needed to fully confirm the long-term material compatibility of the system under varying environmental conditions.

Integrating the results from rheological, NMR, and in situ tests, both formulations showed effective biocidal performance and satisfactory peelability. However, HVPD+C exhibited greater structural stability and homogeneity, with no evidence of phase separation and easier handling during application and removal. HVPD+EO, on the other hand, showed slightly higher elasticity and comparable short-term biocidal activity, though its stability issues may limit reproducibility. Considering all these factors, HVPD+C can be regarded as the more robust and practical formulation for conservation purposes, while HVPD+EO remains an interesting candidate for further studies aimed at improving the sustained release of natural biocidal agents.

In conclusion, this study suggests that the integration of rheology and NMR provides a comprehensive understanding of the structural and functional properties of HVPDs, supporting their development as eco-friendly biocidal systems for cultural heritage conservation. Future efforts should focus on enhancing the formulations' adaptability to challenging conditions while maintaining their biocidal efficacy and environmental sustainability.

Funding sources

This research did not receive any specific grant from funding agencies in the public, commercial, or not-for-profit sectors.

Acknowledgements

The authors wish to express their sincere gratitude to Historic Environment Scotland for granting permission to conduct product testing at Castlelaw Hill Fort. Their support and collaboration have been invaluable in enabling this research and contributing to the study of innovative conservation methods for such culturally significant heritage sites. We are deeply appreciative of their commitment to preserving Scotland's rich history and for providing access to this remarkable archaeological location.

Supplementary materials

Supplementary material associated with this article can be found in the online version at doi:10.1016/j.culher.2025.12.008.

References

[1] Rakesh Kumar, A.V. Kumar, Biodeterioration of Stone in Tropical Environments: An Overview, 1st ed., Getty Publications, 1999.
[2] C. Gaylarde, B. Little, Biodeterioration of stone and metal — Fundamental microbial cycling processes with spatial and temporal scale differences, Sci. Total Environ. 823 (2022) 153193, doi:10.1016/j.scitotenv.2022.153193.
[3] S. Scheerer, O. Ortega-Morales, C. Gaylarde, Chapter 5 Microbial Deterioration of Stone Monuments-An Updated Overview, 66, 1st ed., Elesvier Inc., 2009, doi:10.1016/S0065-2164 (08)00805-8.
[4] Enza Di Carlo, Giovanna Barresi, Palla F, Biodeterioration, Biotechnol. Conserv. Cult. Herit. (2022) 1–30, doi:10.1007/978-3-319-46168-7_1.
[5] L. Tomaselli, G. Lamenti, M. Bosco, P. Tiano, Biodiversity of photosynthetic micro-organisms dwelling on stone monuments, Int. Biodeterior. Biodegrad. 46 (2000) 251–258, doi:10.1016/S0964-8305 (00)00078-0.
[6] T. Warscheid, J. Braams, Biodeterioration of stone: a review, Int. Biodeterior. Biodegrad. 46 (2000) 343–368, doi:10.1016/S0964-8305 (00)00109-8.
[7] Claudia Gazzano, Sergio E Favero-Longo, Paola Iacomussi, R. Piervittori, Biocidal effect of lichen secondary metabolites against rock-dwelling microcolonial fungi, cyanobacteria and green algae, Int. Biodeterior. Biodegrad. 84 (2013) 300–306.
[8] Rachael D Wakefield, M.S. Jones, An introduction to stone colonizing microorganisms and biodeterioration of building stone, Q. J. Eng. Geol. Hydrogeol. 31 (1998) 301–313, doi:10.1144/GSL.QJEG.1998.031.P4.03.
[9] C. Genova, E. Fuentes, P. Sanmartín, G. Favero, B. Prieto, Phytochemical compounds as cleaning agents on granite colonized by phototrophic subaerial biofilms, Coatings 10 (2020) 1–13, doi:10.3390/coatings10030295.
[10] C. Genova, E. Fuentes, G. Favero, B. Prieto, Evaluation of the cleaning effect of natural-based biocides: application on different phototropic biofilms colonizing the same granite wall, Coatings 13 (2023), doi:10.3390/coatings13030520.
[11] L. Rugnini, G. Migliore, F. Tasso, N.T.W. Ellwood, A.R. Sprocati, L. Bruno, Biocidal activity of phyto-derivative products used on phototrophic biofilms growing on stone surfaces of the domus Aurea in Rome (Italy), Appl. Sci. 10 (2020), doi:10.3390/APP10186584.
[12] H.-L. Alakomi, A. Paananen, M.-L. Suihko, I.M. Helander, M. Saarela, Weakening effect of cell permeabilizers on gram-negative bacteria causing biodeterioration, Appl. Environ. Microbiol. 72 (2006) 4695–4703, doi:10.1128/AEM.00142-06.
[13] J.S. Pozo-Antonio, C. Montojo, M.E. López de Silanes, I. de Rosario, T. Rivas, In situ evaluation by colour spectrophotometry of cleaning and protective treatments in granitic Cultural Heritage, Int. Biodeterior. Biodegrad. 123 (2017) 251–261, doi:10.1016/j.ibiod.2017.07.004.
[14] C. Genova, A. Grottoli, E. Zoppis, C. Cencetti, P. Matricardi, G. Favero, An integrated approach to the recovery of travertine biodegradation by combining phyto-cleaning with genomic characterization, Microchem. J. 156 (2020) 104918, doi:10.1016/j.microc.2020.104918.
[15] S. Soltani, A. Shakeri, M. Iranshahi, M. Boozari, A review of the phytochemistry and antimicrobial properties of origanum vulgare L. and subspecies, Iran. J. Pharm. Res. IJPR 20 (2021) 268—285, doi:10.22037/ijpr.2020.113874.14539.
[16] M. Bertuola, N. Fagali, Fernández Lorenzo de Mele M. Detection of carvacrol in essential oils by electrochemical polymerization, Heliyon 6 (2020) e03714, doi:10.1016/j.heliyon.2020.e03714.
[17] S. García-Salinas, H. Elizondo-Castillo, M. Arruebo, G. Mendoza, S. Irusta, Evaluation of the antimicrobial activity and cytotoxicity of different components of natural origin present in essential oils, Molecules 23 (2018), doi:10.3390/molecules23061399.
[18] H. Schulz, G. Özkan, M. Baranska, H. Krüger, M. Özcan, Characterisation of essential oil plants from Turkey by IR and Raman spectroscopy, Vib. Spectrosc. 39 (2005) 249–256, doi:10.1016/j.vibspec.2005.04.009.
[19] F. Palla, M. Bruno, F. Mercurio, A. Tantillo, V. Rotolo, Essential oils as natural biocides in conservation of cultural heritage, Molecules 25 (2020), doi:10.3390/molecules25030730.
[20] M. Stupar, M.L. Grbić, A. Džamić, N. Unković, M. Ristić, A. Jelikić, et al., Antifungal activity of selected essential oils and biocide benzalkonium chloride against the fungi isolated from cultural heritage objects, South African J. Bot. 93 (2014) 118–124, doi:10.1016/j.sajb.2014.03.016.
[21] A. Fraj, F. Jaâfar, M. Marti, L. Coderch, N. Ladhari, A comparative study of oregano (Origanum vulgare L.) essential oil-based polycaprolactone nanocapsules/microspheres: preparation, physicochemical characterization, and storage stability, Ind. Crops Prod. 140 (2019) 111669, doi:10.1016/j.indcrop.2019.111669.
[22] A. Sivropoulou, E. Papanikolaou, C. Nikolaou, S. Kokkini, T. Lanaras, M. Arsenakis, Antimicrobial and cytotoxic activities of *Origanum* essential oils, J. Agric. Food Chem. 44 (1996) 1202–1205, doi:10.1021/jf950540t.
[23] M. Khan, S.T. Khan, M. Khan, A.A. Mousa, A. Mahmood, H.Z. Alkhathlan, Chemical diversity in leaf and stem essential oils of Origanum vulgare L. and their effects on microbicidal activities, AMB Express 9 (2019) 176, doi:10.1186/s13568-019-0893-3.
[24] R. Ranaldi, L. Rugnini, F. Gabriele, N. Spreti, C. Casieri, G. Di Marco, et al., Plant essential oils suspended into hydrogel: development of an easy-to-use protocol for the restoration of stone cultural heritage, Int. Biodeterior. Biodegrad. 172 (2022) 105436, doi:10.1016/j.ibiod.2022.105436.
[25] M. Chelu, Hydrogels with essential oils: recent advances in designs and applications, Gels 10 (2024), doi:10.3390/gels10100636.
[26] L. Giuliani, C. Genova, V. Stagno, L. Paoletti, A.L. Matulac, A. Ciccola, et al., Multi-technique assessment of chelators-loaded PVA-borax gel-like systems performance in cleaning of stone contaminated with copper corrosion products, Gels 10 (2024), doi:10.3390/gels10070455.
[27] E. Boccalon, M. Nocchetti, M. Pica, A. Romani, K. Sterflinger, Hydrogels: a 'stepping stone' towards new cleaning strategies for biodeteriorated surfaces, J. Cult. Herit. 47 (2021) 1–11, doi:10.1016/j.culher.2020.07.008.
[28] A. Tampau, C. González-Martínez, A. Chiralt, Polyvinyl alcohol-based materials encapsulating carvacrol obtained by solvent casting and electrospinning, React. Funct. Polym. 153 (2020) 104603, doi:10.1016/j.reactfunctpolym.2020.104603.

[29] M. Sapper, M. Martín-Esparza, A. Chiralt, C. Gonzalez-Martinez, Antifungal polyvinyl alcohol coatings incorporating carvacrol for the postharvest preservation of golden delicious apple, Coatings 10 (2020) 1027, doi:10.3390/coatings10111027.
[30] J. Andrade, C. González-Martínez, A. Chiralt, The incorporation of carvacrol into poly (vinyl alcohol) films encapsulated in lecithin liposomes, Polymers 12 (2020), doi:10.3390/polym12020497.
[31] M. Palombo, A. Gabrielli, S. De Santis, C. Cametti, G. Ruocco, S. Capuani, Spatio-temporal anomalous diffusion in heterogeneous media by nuclear magnetic resonance, J. Chem. Phys. 135 (2011) 34504, doi:10.1063/1.3610367.
[32] TWC Product and Technology LLC. Weather Underground. 2014 2025. https://www.wunderground.com/.
[33] K. Doudin, M. Lay, S. Al-Malaika, An investigation of the microstructure of PVA polymers using NMR spectroscopic method, Group 2 (2016) G2, doi:10.13140/RG.2.2.34344.98560.
[34] I. Korbag, S. Mohamed Saleh, Studies on the formation of intermolecular interactions and structural characterization of polyvinyl alcohol/lignin film, Int. J. Environ. Stud. 73 (2016) 226–235, doi:10.1080/00207233.2016.1143700.
[35] L. Li, X. Xu, L. Liu, P. Song, Q. Cao, Z. Xu, et al., Water governs the mechanical properties of poly(vinyl alcohol), Polymer 213 (2021) 123330, doi:10.1016/j.polymer.2020.123330.
[36] O.S. Lezova, D.V. Myasnikov, O.A. Shilova, A.G. Ivanova, S.I Selivanov, Study of the composition and structure of ion-conducting membranes based on polyvinyl alcohol by 1H NMR spectroscopy, Int. J. Hydrogen. Energy 47 (2022) 4846–4853, doi:10.1016/j.ijhydene.2021.11.158.
[37] B. Li, Y. Gao, L. Guo, Y. Fan, N. Kawazoe, H. Fan, et al., Synthesis of photoreactive poly (vinyl alcohol) and construction of scaffold-free cartilage like pellets in vitro, Regen. Biomater. 5 (2018) 159–166, doi:10.1093/RB/RBY009.
[38] L.V. Angelova, P. Terech, I. Natali, L. Dei, E. Carretti, R.G. Weiss, Cosolvent gel-like materials from partially hydrolyzed poly(vinyl acetate)s and borax, Langmuir 27 (2011) 11671–11682, doi:10.1021/la202179e.
[39] K. Koumura, K. Satoh, M. Kamigaito, Mn2(CO)10-Induced RAFT polymerization of vinyl acetate, methyl acrylate, and styrene, Polym. J. 41 (2009) 595–603, doi:10.1295/polymj.PJ2009070.
[40] Carretti E., Dei L., Baglioni P. Aqueous polyacrylic acid based gels: physicochemical properties and applications in cultural heritage conservation. In: Miguel M, Burrows HD, Trends Colloid Interface Sci XVI, Berlin, Heidelberg: Springer Berlin Heidelberg; 2004, p. 280–3. https://doi.org/10.1007/978-3-540-36462-7_60.
[41] P. Baglioni, R. Giorgi, D. Chelazzi, Nano-materials for the conservation and preservation of movable and immovable artworks, Int. J. Herit. Digit. Era 1 (2012) 313–318, doi:10.1260/2047-4970.1.0.313.
[42] W. Nosel, S. Capuani, D. Capitani, F. De Luca, Effects of higher rank multipoles on relaxation of an I=3 spin system, J. Magn. Reson. 150 (2001) 178–183, doi:10.1006/jmre.2001.2339.
[43] S. Capuani, F. De Luca, B. Maraviglia, Product-operator formalism in I ≥ 1/2 and S ≥ 3/2 J-coupled nuclear spins: application to J assessment via SEDOR experiment, J. Chem. Phys. 109 (1998) 6564–6570, doi:10.1063/1.477308.
[44] E. Locci, S. Lai, A. Piras, B. Marongiu, A. Lai, 13C-CPMAS and 1H-NMR study of the inclusion complexes of β-cyclodextrin with carvacrol, thymol, and eugenol prepared in supercritical carbon dioxide, Chem. Biodivers. 1 (2004) 1354–1366, doi:10.1002/cbdv.200490098.
[45] B. Gieroba, M. Krysa, K. Wojtowicz, A. Wiater, M. Pleszczyńska, M. Tomczyk, et al., The FT-IR and raman spectroscopies as tools for biofilm characterization created by cariogenic streptococci, Int. J. Mol. Sci. 21 (2020), doi:10.3390/ijms21113811.
[46] J.J. Ojeda, M.E. Romero-Gonzalez, H.M. Pouran, S.A. Banwart, In situ monitoring of the biofilm formation of Pseudomonas putida on hematite using flow-cell ATR-FTIR spectroscopy to investigate the formation of inner-sphere bonds between the bacteria and the mineral, Mineral. Mag. 72 (2008) 101–106, doi:10.1180/minmag.2008.072.1.101.
[47] K. Sizeland, K. Hofman, I. Hallett, D. Martin, J. Potgieter, N. Kirby, et al., Nanostructure of electrospun collagen: do electrospun collagen fibers form native structures? Materialia 3 (2018), doi:10.1016/j.mtla.2018.10.001.
[48] H. K. Sano, T.K.N.H. Kanematsu, T. Tanaka, Corrosion and biofilm for a composite coated iron observed by FTIR-ATR and Raman spectroscopy, Trans. IMF 94 (2016) 139–145, doi:10.1080/00202967.2016.1167315.
[49] S. Ibrahim, A. Ahmad, N.S. Mohamed, Characterization of novel Castor oil-based polyurethane polymer electrolytes, Polymers 7 (2015) 747–759, doi:10.3390/polym7040747.
[50] R. Ellerbrock, H. Gerke, FTIR spectral band shifts explained by OM–cation interactions, J. Plant. Nutr. Soil Sci. 184 (2021), doi:10.1002/jpln.202100056.
[51] S. Cheeseman, Z.L. Shaw, J. Vongsvivut, R.J. Crawford, M.F. Dupont, K.J. Boyce, et al., Analysis of pathogenic bacterial and yeast biofilms using the combination of synchrotron ATR-FTIR microspectroscopy and chemometric approaches, Molecules 26 (2021), doi:10.3390/molecules26133890.
[52] S.J. Parikh, F.N.D. Mukome, X. Zhang, ATR–FTIR spectroscopic evidence for biomolecular phosphorus and carboxyl groups facilitating bacterial adhesion to iron oxides, Colloids Surf. B Biointerfaces 119 (2014) 38–46, doi:10.1016/j.colsurfb.2014.04.022.
[53] S.J. Parikh, J. Chorover, ATR-FTIR spectroscopy reveals bond formation during bacterial adhesion to iron oxide, Langmuir 22 (2006) 8492–8500, doi:10.1021/la061359p.
[54] Y. Ji, X. Yang, Z. Ji, L. Zhu, N. Ma, D. Chen, et al., DFT-calculated IR spectrum amide I, II, and III band contributions of N-methylacetamide fine components, ACS Omega 5 (2020) 8572–8578, doi:10.1021/acsomega.9b04421.
[55] W. Gao, X. Liu, M. Chen, In situ ATR-FTIR investigation and theoretical calculation of the interactions of chromate and citrate on the surface of haematite, RSC Adv. 7 (2017) 41011–41016, doi:10.1039/C7RA04587E.
[56] Marc Boualam Fabienne Quilès LM, Block J-C, Monitoring the effect of organic matter on biofilm growth in low nutritive waters by ATR/FT-IR spectroscopy, Biofouling 18 (2002) 73–81, doi:10.1080/08927010290017752.